UNIVERSIDADE FEDERAL DE VIÇOSA

NATHÁLIA VÁLLERY TOSTES

DNA SIZING, COMPOSITION AND ORIGIN OF INDUCED MICRONUCLEI OF *Zea mays* L.

VIÇOSA - MINAS GERAIS
2021

NATHÁLIA VÁLLERY TOSTES

DNA SIZING, COMPOSITION AND ORIGIN OF INDUCED MICRONUCLEI OF *Zea mays* L.

Dissertação apresentada à Universidade Federal de Viçosa, como parte das exigências do Programa de Pós-Graduação em Genética e Melhoramento, para obtenção do título de *Magister Scientiae*.

Orientador: Wellington Ronildo Clarindo

VIÇOSA - MINAS GERAIS
2021

Ficha catalográfica elaborada pela Biblioteca Central da Universidade Federal de Viçosa - Campus Viçosa

T
T716d
2021

Tostes, Nathália Vállery, 1996-
DNA sizing, composition and origin of induced micronuclei of *Zea mays* L. / Nathália Vállery Tostes. – Viçosa, MG, 2021.
38 f. : il. (algumas color.) ; 29 cm.

Texto em inglês.
Inclui apêndices.
Orientador: Wellington Ronildo Clarindo.
Dissertação (mestrado) - Universidade Federal de Viçosa.
Referências bibliográficas: f. 29-35.

1. Milho - Melhoramento genético. 2. Mutagênese. 3. Sequenciamento de nucleotídeo. 4. Micromanipulação. 5. DNA. I. Universidade Federal de Viçosa. Departamento de Biologia Geral. Programa de Pós-Graduação em Genética e Melhoramento. II. Título.

CDD 22. ed. 633.152

NATHÁLIA VÁLLERY TOSTES

DNA SIZING, COMPOSITION AND ORIGIN OF INDUCED MICRONUCLEI OF *Zea mays* L.

Dissertação apresentada à Universidade Federal de Viçosa, como parte das exigências do Programa de Pós-Graduação em Genética e Melhoramento, para obtenção do título de *Magister Scientiae*.

APROVADA: 12 de fevereiro de 2021.

Assentimento:

Nathália V. Tostes
Nathália Vállery Tostes
Autora

Wellington Ronildo Clarindo
Orientador

Aos meus pais Rosana e Milton
Ao meu irmão Gustavo
Dedico

AGRADECIMENTOS

À Universidade Federal de Viçosa e ao Programa de Pós-Graduação em Genética e Melhoramento pela infraestrutura fornecida e pela oportunidade de realização do curso.

Ao professor Wellington Clarindo pela orientação, amizade e conhecimentos compartilhados.

Ao professor Leonardo Bhering pelo auxílio nas análises estatísticas.

À banca examinadora, composta pelas professoras Larissa Vieira, Milene Praça-Fontes e Tatiana Souza, pelas valiosas considerações e sugestões.

A todos os professores que me ofereceram valiosos ensinamentos ao longo da minha formação.

Aos meus pais Rosana e Milton, que nunca mediram esforços para me apoiar e incentivar minhas escolhas, que são meus exemplos de força e dedicação e a quem devo essa conquista. Ao meu irmão Gustavo, que mesmo com seu jeito torto sempre me apoiou e esteve ao meu lado. À Nina, Valentina e Isadora, que são minhas fiéis parceiras e a representação do amor mais puro e leal.

A todos os colegas e parceiros do laboratório de Citogenética e Citometria, pela amizade, apoio e momentos de descontração. Em especial à Jéssica e Fernanda pelo auxílio na condução dos experimentos, e à Luana e Mariana pelas longas conversas.

A Deus por todas as bençãos e por sempre guiar meus caminhos.

O presente trabalho foi realizado com apoio da Coordenação de Aperfeiçoamento de Pessoal de Nível Superior – Brasil (CAPES) – Código de Financiamento 001.

“Nothing in life is to be feared,
it is only to be understood.”
(Marie Curie)

ABSTRACT

TOSTES, Nathália Vállery, M.Sc., Universidade Federal de Viçosa, February, 2021. **DNA sizing, composition and origin of induced micronuclei of *Zea mays* L.** Advisor: Wellington Ronildo Clarindo.

Micronuclei (MN) are constituted of chromatin, which originated from DNA damages induced by mutagens. The mutagens promote a clastogenic effect characterized by chromosome structure damage, and/or an aneugenic effect with the loss of a whole chromosome. Due to their origin, MN are distinct in relation to genomic origin and composition. In plant mutagenesis, centromeric, telomeric and rDNA sequences were identified in MN composition. We aimed to investigate the DNA sizing, composition and origin of induced *Zea mays* MN after methyl methanesulfonate (MMS) treatment. Using image cytometry, we showed that the MN have distinct DNA sizing, predominantly between 0.5 – 1.5 pg. These values indicated that the MN were generated from different chromosome fragments. The variability of MN composition was confirmed by fluorescence signal variation of 180-bp knob and *Grande* LTR-retrotransposon sequences. Therefore, these sequences, especially the *Grande* LTR-retrotransposon sequence that is rich in guanine, can be considered hotspots of MMS damage and, consequently, for MN formation. The different MN origins were also revealed by a probe pool produced from two individual microdissected MN. Each microdissected MN was originated from different chromosome fragments consisting of DNA sequences of all *Z. mays* chromosomes. Altogether, our results showed the variability of *Z. mays* MN from several chromosome fragments formed after MMS treatment. Therefore, our findings demonstrated the extent of the genotoxic damage promoted by MMS in *Z. mays* genome. We provided insights concerning the structure of MN and methodologies that can be employed in plant mutagenesis research.

Keywords: Mutagenesis. Maize. DNA content. Microdissection. Repetitive DNA sequences.

RESUMO

TOSTES, Nathália Vállery, M.Sc., Universidade Federal de Viçosa, fevereiro de 2021. **Tamanho do genoma, composição e origem de micronúcleos induzidos de *Zea mays* L.** Orientador: Wellington Ronildo Clarindo.

Os micronúcleos (MN) são constituídos por cromatina, que se originam de danos ao DNA induzidos por agentes mutagênicos. Os agentes mutagênicos promovem um efeito clastogênico caracterizado por danos à estrutura cromossômica e/ou um efeito aneugênico com a perda de um cromossomo inteiro. Devido à sua origem, os MN são distintos em relação à origem genômica e composição. Na mutagênese vegetal, sequências centroméricas, teloméricas e de rDNA foram identificadas na composição de MN. Nosso objetivo foi investigar o tamanho do DNA, composição e origem de MN induzidos de *Zea mays* após o tratamento com metanossulfonato de metila (MMS). Usando citometria de imagem, mostramos que os MN possuem tamanhos de DNA distintos, predominantemente entre 0,5 - 1,5 pg. Esses valores indicaram que os MN foram gerados a partir de fragmentos cromossômicos diferentes. A variabilidade da composição dos MN foi confirmada pela variação do sinal de fluorescência das sequências knob 180-bp e do retrotransposon-LTR *Grande*. Portanto, essas sequências, principalmente a sequência retrotransposon-LTR *Grande* rica em guanina, podem ser consideradas hotspots de danos por MMS e, consequentemente, de formação de MN. As diferentes origens dos MN também foram reveladas por um pool de sondas produzido a partir de dois MN individuais micromanipulados. Cada MN micromanipulado foi originado de diferentes fragmentos de cromossomos que consistem em sequências de DNA de todos os cromossomos de *Z. mays*. No geral, nossos resultados mostraram a variabilidade de MN de *Z. mays* a partir de vários fragmentos de cromossomos formados após o tratamento com MMS. Portanto, nossos resultados demonstraram a extensão do dano genotóxico promovido por MMS no genoma de *Z. mays*. Fornecemos insights sobre a estrutura dos MN e metodologias que podem ser empregadas na pesquisa de mutagênese vegetal.

Palavras-chave: Mutagênese. Milho. Conteúdo de DNA. Micromanipulação. Sequências repetitivas de DNA.

SUMÁRIO

RESEARCH PAPER: DNA SIZING, COMPOSITION AND ORIGIN OF INDUCED MICRONUCLEI OF *Zea mays* L.

Nathália Vállery Tostes[a], Fernanda Aparecida Ferrari Soares[a], Jéssica Coutinho Silva[a], Leonardo Lopes Bhering[b], Wellington Ronildo Clarindo[a*]

[a]Laboratório de Citogenética e Citometria, Departamento de Biologia Geral, Universidade Federal de Viçosa, 36.570-900 Viçosa, MG, Brazil.
[b]Laboratório de Biometria, Departamento de Biologia Geral, Universidade Federal de Viçosa, 36.570-900 Viçosa, MG, Brazil.

*Corresponding author: well.clarindo@ufv.br

1. Introduction

Micronuclei (MN) are cell structures that originate from chemical, physical or biological mutagens. MN are small extranuclear structures resulting from clastogenic and/or aneugenic effects (Figure 1). Clastogenic agents promote lesions in the DNA double strand and the inhibition of the DNA damage repair system, resulting in structural chromosome alterations and/or chromosome bridges (Fenech et al., 2011). As a result of the clastogenic effect, MN are generated from acentric chromosome fragments (Kirsch-Volders et al., 2011). The aneugenic effect is characterized by the loss of a whole chromosome, which does not attach to the spindle fibers during mitotic/meiotic metaphases causing anaphase segregation errors (Terradas et al., 2010). Defects in microtubule-kinetochore connections promote the aneugenicity as a consequence of cytosine hypomethylation in centromeric DNA (Gieni et al., 2008; Heit et al., 2009), incorrect mitotic spindle assembly (Gisselsson, 2008), errors in cell cycle check points (Guo et al., 2019) and/or abnormal centrosome duplication (Zyss and Gergely, 2009). The resulting chromosome fragments or lagging chromosomes are delimited by the nuclear envelope separately of the main nucleus at the end of telophase, generating the MN (Fenech et al., 2011; Kirsch-Volders et al., 2011).

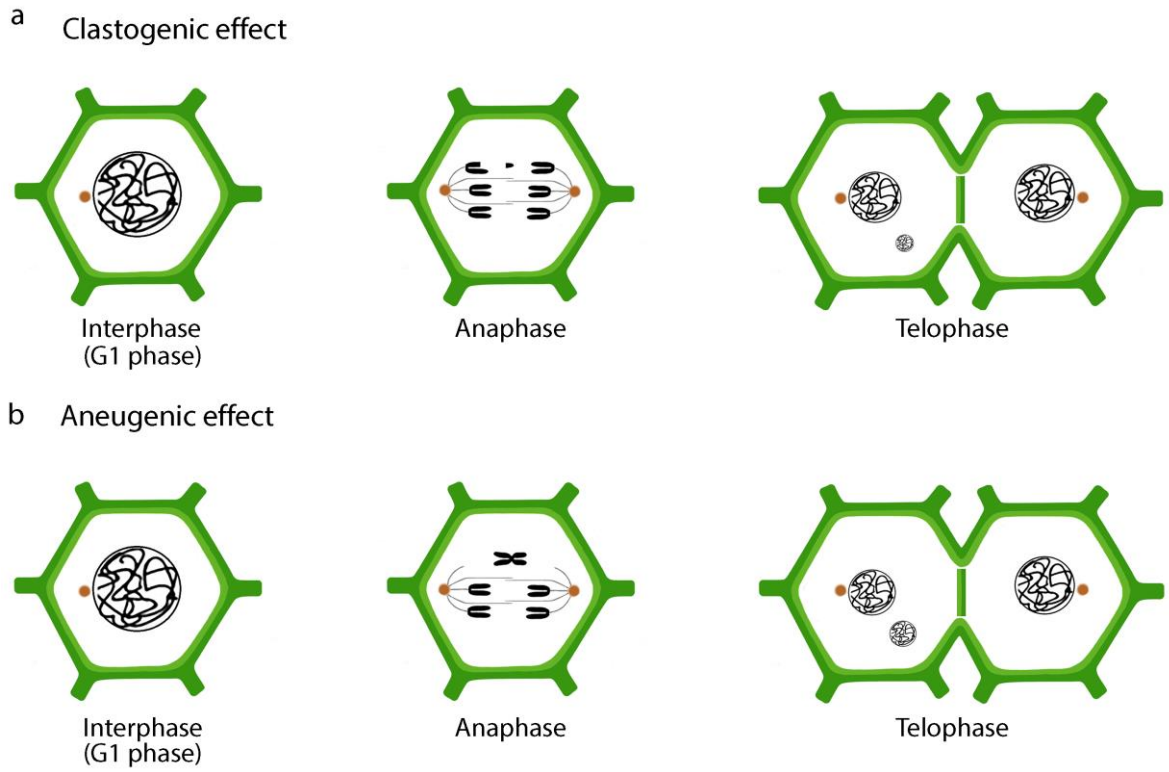

Figure 1. Representative scheme of the MN formation pathways. **(a)** The clastogenic effect promotes chromosomal fragmentation. **(b)** The aneugenic effect impedes a whole chromosome to attach to the spindle fibers. The MN result from these fragments and/or lagging chromosomes at the telophase end.

MN can have different fates according to their formation pathways, genomic composition, cell type and species (Hintzsche et al., 2017). The possible fates for these structures include degradation of the MN, reincorporation into the main nucleus, extrusion from the cell, persistence in the cytoplasm, premature chromosome condensation/chromothripsis and elimination by apoptosis (Hintzsche et al., 2017). Due to MN formation pathways and their possible persistence in the cytoplasm, MN frequency is widely used to evaluate the possible mutagenic potential, evidencing the genotoxic effects of different agents in animals (Leveroni et al., 2017; Itoh and Hattori, 2019), humans (Wang et al., 2017) and plants (Alvarenga et al., 2020; Chen et al., 2020).

Considering that MN can be originated from chromosome fragments or whole chromosomes, these structures can have different DNA sizing (Nüsse et al., 1996). Besides, since MN can persist in a cell or be lost, it is relevant to know how much

DNA the MN carries. Thus, identifying the difference between the nuclear and micronuclear DNA sizing gives additional information on the extent of the damage promoted by genotoxic agents.

DNA sizing measurement in plants (Pellicer and Leitch, 2020) and animals (Gregory, 2021) is usually accomplished using flow cytometry. The DNA sizing of MN from mouse fibroblasts was investigated using flow cytometry after treatment with tear gas chlorobenzylidene malonitrile (Miller and Nússe, 1993; Nüsse et al., 1996), vinblastine (Nüsse et al., 1996) and γ radiation (Nüsse et al., 1992; Nüsse et al., 1996). These studies showed the MN population and its large variation in relation to DNA sizing by biparametric histograms (Side-scattered light – SSC *x* fluorescence intensity). From the biparametric histograms, the DNA sizing variation was compared to the DNA sizing of the chromosomes, which was measured through flow karyotyping. Based on DNA sizing values (MN and mice chromosomes), the authors appointed the MN origin from chromosome fragments or whole chromosomes. In plant mutagenesis, the MN DNA sizing has not been measured. An investigation of MN DNA sizing in plants using flow cytometry presents some obstacles, such as the separation of the MN from the cellular wall debris and organelles, like mitochondria and plastids. In addition, flow cytometry requires a large amount of particles with the same C value to obtain a histogram which allows the recognition of the DNA sizing (Doležel et al., 2007). As MN can present different DNA contents as a consequence of their origin, the DNA sizing of these structures is a challenge. In this scenario, image cytometry is an alternative approach for MN DNA measurement. Image cytometry has advantages over flow cytometry since it allows the visual recognition of the nuclei (Rodenacker and Bengtsson, 2003) and the analysis is possible with a small number of nuclei (Greilhuber, 2008).

The composition of MN has been investigated via the verification of the presence of DNA sequences from particular chromosomes and chromosome portions. Human lymphocytes treated with physical (γ ray radiation, Fimognari et al., 1997) and chemical mutagens (5-azacytidine, Guttenbach and Schmid, 1994; mitomycin C, diethylstilbestrol, Fauth et al., 2000; and 1,2,4-benzenetriol, Chung et al., 2002) provided MN composed of sequences originating from different human chromosomes. The treatment of human leukocytes with mitomycin C (Hovhannisyan et al., 2012) corroborated the previous results. Similarly, the MN from root tip

meristematic cells of *Hordeum vulgare* L. (Jovtchev et al., 2002; Juchimiuk et al., 2007; Juchimiuk-Kwasniewska et al., 2011) and *Brachypodium distachyon* (L.) P. Beauv. (Kus et al., 2017; Kus et al., 2018; Kus et al., 2019), which were treated with chemical (N-nitroso-N-methylurea and maleic hydrazide) and physical mutagens (γ and X ray radiation), presented centromeric, telomeric, 5S and 25S rDNA sequences.

Plant genomes present repetitive DNA sequences, like tandem repeats and mobile elements (Lee and Kim, 2014). Moreover, regions composed by repetitive DNA sequences are considered hotspots for the occurrence of structural chromosomal rearrangements. Heterochromatic regions exhibiting repetitive DNA sequences (Schubert et al., 1994), mobile elements (Lysák and Schubert, 2013) or 180-bp knob sequences (Silva et al., 2020) were identified as regions prone to suffer chromosome rearrangements, especially deletions. Therefore, it is possible that these sequences can be involved in MN composition. Tandem repeated sequences (centromeric, telomeric, 5S and 25S rDNA sequences) have been identified in MN of *H. vulgare* (Juchimiuk et al., 2007; Juchimiuk-Kwasniewska et al., 2011) and *B. distachyon* (Kus et al., 2017; Kus et al., 2018). Since the identification of repetitive DNA sequences contributes to the understanding of structure and organization of the nuclear genome (Wang et al., 2006), it is required to verify the presence of these sequences in MN composition.

Together with the MN composition, understanding the MN origin can also help to elucidate questions concerning their structure and organization. The construction of probes from microdissected MN can be employed to reveal the origin of the MN (Engelen et al., 1998). A spontaneous micronucleus in human lymphocytes was microdissected and its DNA was amplified by RAPD-PCR. From fluorescent *in situ* hybridization (FISH), the micronucleus DNA probe evidenced that the micronucleus originated from chromosome 2 (Peace et al., 1999). To our knowledge, a study aiming to find out the MN origin was until now not conducted in plant mutagenesis.

Zea mays L. is a species with a relatively well-characterized genome, and with sequencing data available from public domain databases (Schnable et al., 2009). The *Z. mays* genome consists of ~85% of mobile elements, which were characterized (Schnable et al., 2009) and mapped (Mroczek and Dawe, 2003; Lamb et al., 2007; Silva et al., 2020). Besides, procedures for chromosome DNA sizing

(Silva et al., 2018) and for construction of specific probes from microdissection (Soares et al., 2020) and repetitive DNA sequences (Silva et al., 2020) are available for *Z. mays*.

Increased knowledge on DNA and chromosomal damages contributes to the understanding of the biological impact level promoted by genotoxic agents (Kus et al., 2017). In light of this, we aimed to investigate the DNA sizing, composition and origin of induced MN in *Z. mays*. We propose the use of image cytometry for DNA measurement, FISH with 180-bp knob sequence and *Grande* LTR-retrotransposon probes and microdissection to realize these analyses.

2. Materials and methods

2.1. Plant material and micronuclei induction

Commercial seeds of *Z. mays* 'AL Bandeirante' (Sementes Caiçara®, allotment seed number 91, category S2, harvest 2016, germination rate of 94.0%, 99.5% purity) were germinated in Petri dishes on filter paper moistened with dH_2O at 30ºC. Methyl methanesulfonate (MMS, Sigma – Aldrich®, CAS No 66-27-3) is a chemical mutagen able to cause DNA damage like breaks and adducts, which are expressed as chromosomal rearrangements (Lundin et al., 2005). Based on the MMS concentration usually used as positive control in mutagenesis studies, mostly with *Allium cepa* L. (4×10^{-4} M, Caritá and Marin-Morales, 2008; Leme and Marin-Morales, 2008; De Grippa et al., 2010; Lima et al., 2019), we used an overdose of MMS to induce a high frequency of MN. For this, roots with 1 cm length were transferred to Petri dishes containing 2×10^{-3} M MMS solution and incubated for 24 h at 30ºC (~20 seeds/Petri dish). Noteworthy, we also tested higher doses than the one used here which turned out lethal to the biological material. Roots germinated only in dH_2O were used as negative control. The root tips were washed in dH_2O, fixed three times in 3:1 methanol: acetic acid (Merck®) with changes after each 10 min and stored at -20ºC.

2.2. Micronuclear DNA sizing by image cytometry

After 24 h in methanol:acetic acid fixative solution, the roots used for image cytometry were transferred to 95% ethanol and stored at -20ºC for 24 h. The roots were washed three times in dH_2O, macerated in enzymatic pool (4% cellulase Sigma®, 0.4% hemicellulase Sigma®, 1% macerozyme Onozuka R10 Yakult®, 100% pectinase Sigma®) diluted in dH_2O in the proportion 1:8 (enzyme pool:dH_2O) for 2 h at 36ºC, washed three times with dH_2O, fixed three times in 95% ethanol with changes after each 10 min and stored at -20ºC for 24 h (Silva et al., 2018). The slides were prepared using the squashing technique. On the same slide, MMS root meristems and dH_2O root meristems (negative control) were squashed on opposite sides in order for both of them to receive the exactly same Feulgen reaction condition. The slides were frozen at -80ºC for 10 min, the coverslips were removed and immediately incubated for 12 h in 17:5:1 methanol:formaldehyde:acetic acid (Merck®) at 25ºC. Next, the slides were washed in dH_2O, air-dried and hydrolyzed in 5 M HCl (Merck®) for 40 – 50 min at 25ºC, washed in dH_2O, air-dried, and stained with Schiff's reagent (Hardie et al., 2002) for 12 h at 4ºC. Subsequently, the slides were washed in 0.5% SO^{2-}water (Merck®) for 3 min and two times in dH_2O for 3 min (Carvalho et al., 2011).

The setup and calibration of the microscope and image analysis system were performed to measure the optical density (OD) and the integrated optical density (IOD) values (Hardie et al., 2002; Carvalho et al., 2011). The software algorithm automatically calculated the IOD values multiplying the nuclear area of the nuclei or the MN (μm^2) by the mean OD. Ten slides were prepared and for each of them ten frames were randomly captured, once for the MMS treatment and once the negative control, resulting in 200 frames for each treatment. The frames were captured using a 12-bit CCD digital video camera (Olympus® DP71) coupled to a trinocular photomicroscope Olympus™ BX-60, equipped with stabilized light source, UPlanFI objective with magnification ×100, 1.4 numeric aperture, aplanat achromat condenser with 1.4 aperture, and neutral density filter (ND6). Based on recommendations for DNA measurement through image cytometry by Vilhar et al. (2001), ten MN, ten early prophasic and ten late telophasic nuclei were digitally segmented, each frame using the Image Pro-Plus® 6.1 analysis system (Media

Cybernetics®). The early prophases and late telophases were used because it is visually possible to recognize them and mainly to define their ploidy levels.

We calculated the IOD for each prophasic and telophasic nuclei and then we calculated the mean IOD for each slide. From these values, we calculated the 4C/2C ratio, coefficient of variation (CV) and standard deviation for each slide for image cytometry quality control (Böcking and Huy Nguyen, 2004; Haroske et al., 2001; Vilhar et al., 2001). For each slide, the IOD was also calculated for each MN. Based on the mean IOD from telophasic nuclei (the same for prophasic nuclei), the IOD from each MN and considering the nuclear DNA sizing of *Z. mays* 'AL Bandeirante' 2C = 6.10 pg (Silva et al., 2018), we calculated the DNA sizing from each MN using the formula:

$$MN\ pg = \frac{IOD\ MN\ x\ 6{,}10\ pg}{mean\ IOD\ telophase}.$$

The MN DNA sizing values were submitted to a descriptive statistical analysis using Rbio software (Bhering, 2017) to group MN with similar DNA sizing.

2.3. Probe construction

MN composition was investigated using probes of 180-bp knob and *Grande* LTR-retrotransposon sequences. These sequences were used due to their occurrence in the *Z. mays* genome. The probe of 180-bp knob sequence was generated via PCR, as performed by Silva et al. (2020), using the primers *F* 5′-ATAGCCATGAACGACCATTT-3′ and *R* 5′-ACCCCACATATGTTTCCTTG-3′ (Fourastié et al., 2018). The *Grande* LTR-retrotransposon probe was amplified from the primers *F* 5′-ATGCGAGGATAAGTCGGCGAAG-3′ and *R* 5′-GGTGTTTTTAGGAGTAGGACGGTG-3′ (Mroczek and Dawe, 2003).

To verify the origin of the MN, we separately microdissected five MN and generated a specific probe pool from their genomic DNA. For this, we prepared slides using the macerated root meristems of the MMS treatment. Each meristem was dissociated under the slide, and the slides were immediately immersed in dH_2O for 1 min to keep the MN hydrated and to allow the material removal without chromatin fragment loss. The microdissections were carried out using an Eppendorf TransferMan® micromanipulator coupled to an inverted phase contrast microscope

IX70 (Olympus™) in a room at a relative humidity of ~70%. The slides were visualized with an objective LUCPlanFLN UIS 2 60X/0.70 Ph2 and the five MN were microdissected using sterile Femtotips (Eppendorf®) glass microneedles. These different MN were individually transferred to sterile microtubes of 0.2 mL containing 0.1 mL of sterile collection solution (10 mM Tris–HCl pH 7.5 + 10 mM NaCl + 1 mM EDTA + 0.1% SDS + 0.1% Triton X-100 + 30% Glycerol +1.44 mg mL^{-1} Proteinase-K, Sigma®). Immediately, the MN were deproteinized for 2 h at 60ºC, followed by enzyme inactivation at 80ºC for 20 min (adapted from Yang et al., 2017). All steps were conducted in UV-irradiated biohazard flow chambers, and the pipetting procedures were carried out with tips containing sterile filters in order to avoid contamination (Soares et al., 2020).

After the Proteinase-K treatment, the genomic DNA of each MN was amplified and labeled by PCR using a DOP primer 5'-CCGACTCGAGNNNNNNATGTGG-3' (Telenius et al., 1992). DNA amplification was accomplished in two rounds (Yang et al., 2017; Soares et al., 2020). The first amplification reaction mix consisted of the deproteinized MN DNA, 4 µM DOP, 200 µM of each dNTP (Promega®), 1X Thermo Sequenase DNA Polymerase (GE®) reaction buffer and 20X Thermo Sequenase DNA Polymerase (GE®). The PCR conditions were initial denaturation at 95ºC for 3 min; 10 cycles of 92°C for 1 min; 35°C for 2 min; ramp of 0.1°C/s until 72°C; 72°C for 1:30 min; 30 cycles of 92°C for 1 min; 56°C for 2 min; 72°C for 2 min and final extension at 72°C for 5 min. The second amplification reaction mix consisted of 200 ng of the amplified MN DNA, 4 µM DOP, 200 µM of each dNTP (Promega®), 1X Thermo Sequenase DNA Polymerase (GE®) reaction buffer and 20X Thermo Sequenase DNA Polymerase (GE®). The PCR conditions were initial denaturation at 96ºC for 3 min; 30 cycles of 91°C for 1 min; 56°C for 1 min; ramp of 0.1°C/s until 72°C; 72°C for 2 min and final extension at 72°C for 5 min. The amplification products were visualized by electrophoresis in 1.5% agarose gel. Based on differences between the amplified sequence sizes, we chosen two genomic MN, which were denominated as MN 1 and MN 2 (Supplementary Figure 1). The labeling reaction for the probe pool construction consisted of 200 ng of the amplified DNA, 4 µM DOP, 200 µM each of dATP, dCTP and dGTP, 100 µM dTTP, 1X Thermo Sequenase DNA Polymerase (GE®) reaction buffer, 20X Thermo Sequenase DNA Polymerase (GE®) and 50 µM fluorochromes ChromaTide® Alexa Fluor® 488-5-dUTP (Life

Technologies®) for MN 1 and Tetramethyl-rhodamine 5-dUTP (Roche®) for MN 2. The amplification conditions for the labeling reaction were identical to the second round described above. All amplification and labeling mixes were prepared in UV-irradiated flow chambers, using sterile pipettes and tips with filter, to avoid DNA contamination.

2.4. Composition and origin of the micronuclei

We verified the occurrence of 180-bp knob and *Grande* LTR-retrotransposon sequences in nuclei and MN. For this, roots treated with MMS and enzymatically macerated, performed as described in the section "*Micronuclear DNA sizing by image cytometry*", were fixed in 3:1 methanol:acetic acid. Slides were prepared from the cellular dissociation of these roots and air-dried (Silva et al., 2020).

In addition, slides with metaphasic chromosomes were used to map the 180-bp knob and *Grande* LTR-retrotransposon sequences and to verify the origin of the microdissected MN. For these, seeds were germinated in dH_2O, and the 1 cm roots were incubated at 30ºC for 18 h in solution of 1.75 mM hydroxyurea (Sigma®) and 0.20 g L^{-1} MS salts (Sigma®) for synchronization of the cell cycle. The roots were washed for 1 h in dH_2O at 30ºC with changes every 15 min for cell cycle recovery. For metaphase arresting, the roots were treated with 3 µM amiprophos-methyl (Sigma®) in 0.3% dimethyl sulfoxide (Sigma®) for 4 h at 30°C. The roots were washed in dH_2O and fixed three times in 3:1 methanol:acetic acid with changes after each 10 min and stored at -20ºC. The roots were washed three times in dH_2O, submitted to enzymatic maceration as described in the section "*Micronuclear DNA sizing by image cytometry*", washed in dH_2O, fixed in 3:1 methanol:acetic acid with three changes after 10 min, and stored at −20°C. Slides were prepared by cellular dissociation and air-drying techniques. Slides with morphologically preserved metaphases, nuclei and MN were aged for at least 5 days (Silva et al., 2020).

The slides were washed in 1X PBS buffer for 5 min, fixed with 4% formalin for 15 min, washed again in 1X PBS for 5 min, and dehydrated in cold ethanol series (70%, 85% and 100%) for 5 min each. For the 180-bp knob and *Grande* LTR-retrotransposon probes, the hybridization mix consisted of 50% formamide (Sigma®) + 2X SSC (Sigma®), 35 µg competitor DNA (Herring Sperm DNA, Promega®) and

100 ng of the probe (Silva et al., 2020). For the MN probe pool, the hybridization mix consisted of 50% formamide (Sigma®) + 2X SSC (Sigma®), 20 µg competitor DNA (Herring Sperm DNA, Promega®), 200 ng extra competitor DNA (amplified DNA from MN 1 for MN 2 probe pool and conversely) and 200 ng of the probe pool. The mixes were denatured at 85°C for 5 min, followed by immediate transfer to ice for at least 5 min. 35 µL of the mix were placed on the slides, which were covered by a plastic coverslip HybriSlip (Sigma®) and sealed with Rubber Cement Elmer's®. In a ThermoBrite system (ThermoFisher®), nuclei and MN were denatured at 68ºC for 3 min and metaphases at 70°C for 3 min, followed by hybridization at 37°C for 24 h. After, the coverslips were removed and stringency washes were performed in three solutions of 50% formamide/2X SSC and one of 2X SSC, for 5 min each at 45°C, resulting in a stringency of ~82%. The slides were counterstained with 40% glycerol/PBS + 6-diamidino-2 phenylindole (DAPI), covered with 24 x 40 mm glass coverslip and sealed with nail polish (adapted from Schwarzacher and Heslop-Harrison, 2000). The MN images obtained from DAPI counterstaining were also used to investigate the presence of AT rich-portions in the MN composition.

For each probe, at least 15 metaphases and at least 20 nuclei with MN were randomly captured with a photomicroscope Olympus™ BX60 equipped with an immersion objective 100x/A.N. 1.4, a 12-bits CCD digital video camera (Olympus™ DP71), WB (MN 1 probe pool – green florescence), WG (MN 2 probe pool, 180-bp knob and *Grande* LTR-retrotransposon probes – red florescence) and WU (DAPI staining) filters, and a computer with a digitizer plate. The images were captured using the exposure time of 1/1.8 sec for green and red florescence and 1/60 sec for DAPI staining, processed by Image ProPlus 6.1 software (Media Cybernetics®) and edited with the same brightness and contrast in Adobe Photoshop CC.

3. Results

The hydrolysis from 5 M HCl for 45 min provided morphologically preserved nuclei and MN, without cytoplasmic background and stoichiometrically stained by Schiff's reagent (Supplementary Figure 2). System calibration was appropriate, since the obtained 4C/2C ratio, CV and standard deviation values were adequate. The 4C/2C ratio oscillated from 2.054 – 2.175; required optimum values lie between

1.8 and 2.2 (Böcking and Huy Nguyen, 2004). CV ranged from 2.533% – 4.538% for prophasic and 2.347% – 4.861% for telophasic nuclei. CV values for image cytometry analyses must be lower than 5% (Haroske et al., 2001). Standard deviations ranged from 4.769 – 18.835 for prophasic and 2.437 – 13.249 for telophasic nuclei. Thus, we considered the image cytometry procedure adequate to measure the IOD values of the nuclei and MN.

The IOD mean values for the slides ranged from 187.476 – 591.728 for prophasic and from 86.383 – 272.536 for telophasic nuclei, highlighting the relevance of the presence of the MMS treated meristematic cells and of the negative control in the same slide. Each MN showed a distinct IOD value, which varied for each slide. They ranged from 18.168 – 23.207; 24.941 – 39.494; 14.362 – 34.169; 16.317 – 38.297; 19.861 – 43.051; 19.345 – 45.624; 24.941 – 41.647; 11.753 – 42.259; 11.776 – 42.960; 13.882 – 68.086, showing the variability of the MN in relation to the DNA sizing (Figure 2). Consequently, the DNA sizing values from each MN were distinct. The variation of MN DNA sizing was categorized in 6 groups (Figure 3). The majority of the MN (69%) presented DNA sizing ranging from 0.5 – 1.5 pg (groups 2 and 3). Whereas, MN with DNA sizing ranging from 2.0 – 3.0 pg (groups 5 and 6) were less frequent (4%).

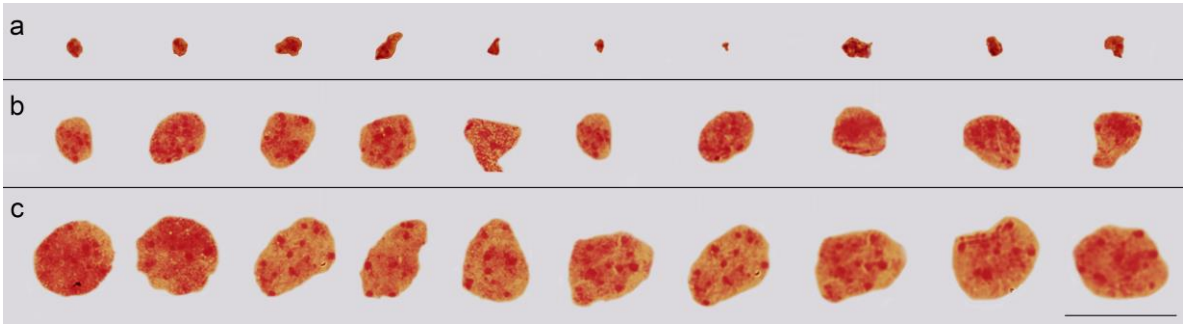

Figure 2. Representative collection of **(a)** MN, **(b)** telophasic and **(c)** prophasic nuclei of *Z. mays* obtained from the same slide. Bar = 10 µm.

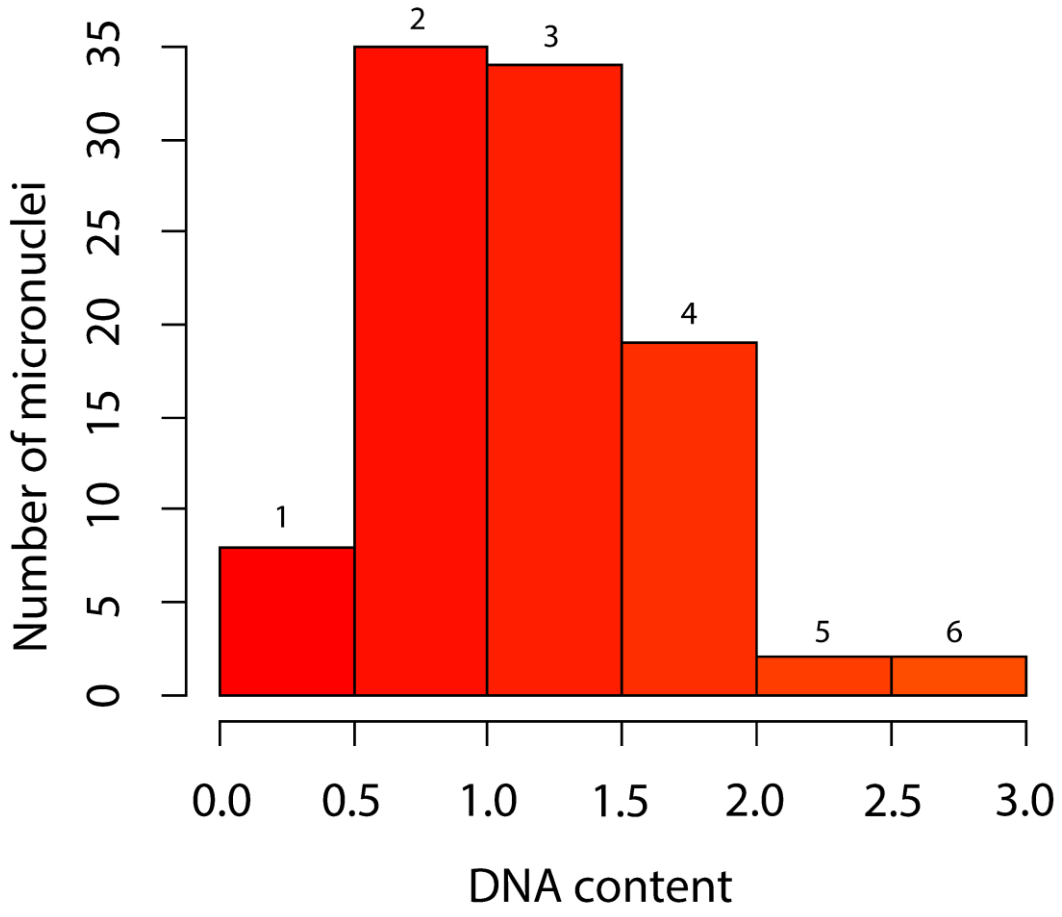

Figure 3. Representative histogram of the MN DNA sizing values in pg. The MN DNA sizing presented variable values, which were categorized in groups 1, 2, 3, 4, 5 and 6 according to their respective intervals of DNA sizing. A predominance of MN with 0.5 – 1.5 pg was observed.

180-bp knob and *Grande* LTR-retrotransposon sequences were also found in the MN composition. 180-bp knob sequence exhibited disperse signals in MN with a variation of fluorescence signals obtained in each MN (Figure 4a). In metaphases, positive signals were visualized in the long arm of the chromosomes 1, 2, 4, 5 and 8 and in the short arm of the chromosome 5, with heterozygosity in pairs 1 and 5 (Figure 5a). We found scattered signals of the *Grande* LTR-retrotransposon sequence with variable distribution in each MN (Figure 4b). Moreover, strong uniform signals were observed along the length of the ten chromosomes (Figure 5b). From MN counterstained with DAPI, a variation of positive signals was presented, showing

that AT rich-regions are involved in MN composition (Figure 6), and indicating that the MN presented chromatin with different compaction levels.

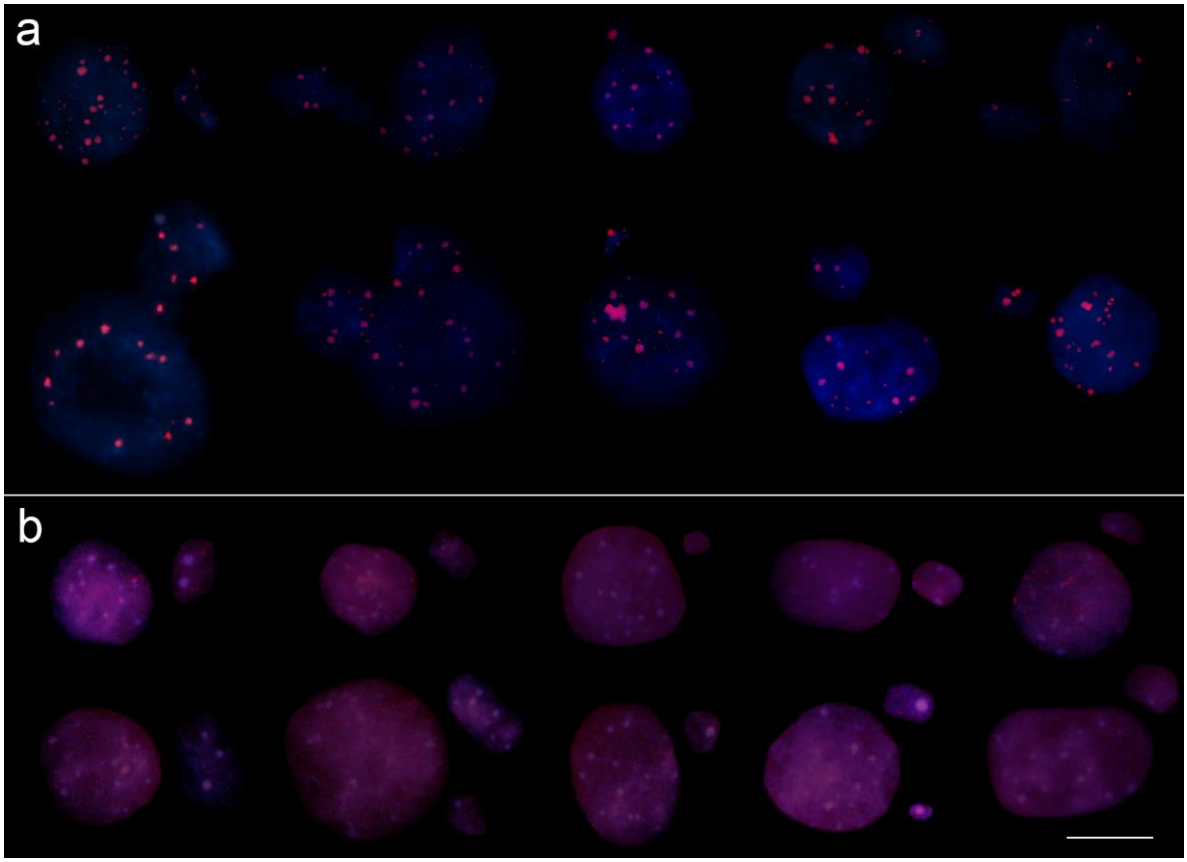

Figure 4. Composition of nuclei/MN of *Z. mays* from *in situ* hybridization from probes labelled with Tetramethyl-rhodamine 5-dUTP (red) of **(a)** 180-bp knob and **(b)** *Grande* LTR-retrotransposon sequences. **(a)** Hybridization signals were observed dispersed along the nuclei/MN with variation of signal intensity in each MN. **(b)** MN displaying scattered hybridization signals with variable distribution and intensity in each MN. Bar = 10 µm.

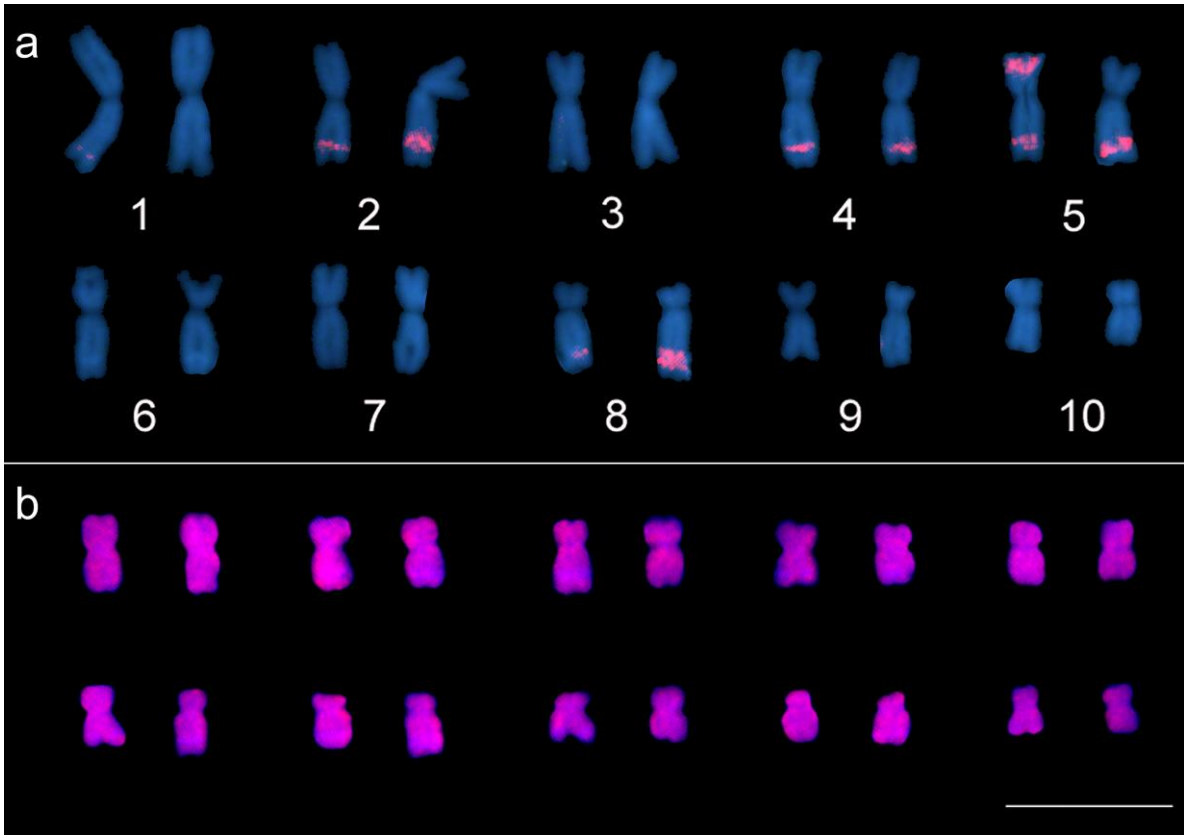

Figure 5. Mapping of the **(a)** 180-bp knob and **(b)** *Grande* LTR-retrotransposon sequences (Tetramethyl-rhodamine 5-dUTP – red fluorescence) in the *Z. mays* karyotype. **(a)** Hybridization signals were mapped in the long arm of the chromosomes 1, 2, 4, 5 and 8, exhibiting heterozygosity in the chromosome pairs 1 and 5. This result shows that the MN possess sequences of these *Z. mays* chromosomes. **(b)** All chromosomes displayed hybridization signals evenly distributed, indicating that the MN may be composed of fragments of the ten *Z. mays* chromosomes. Bar = 10 µm.

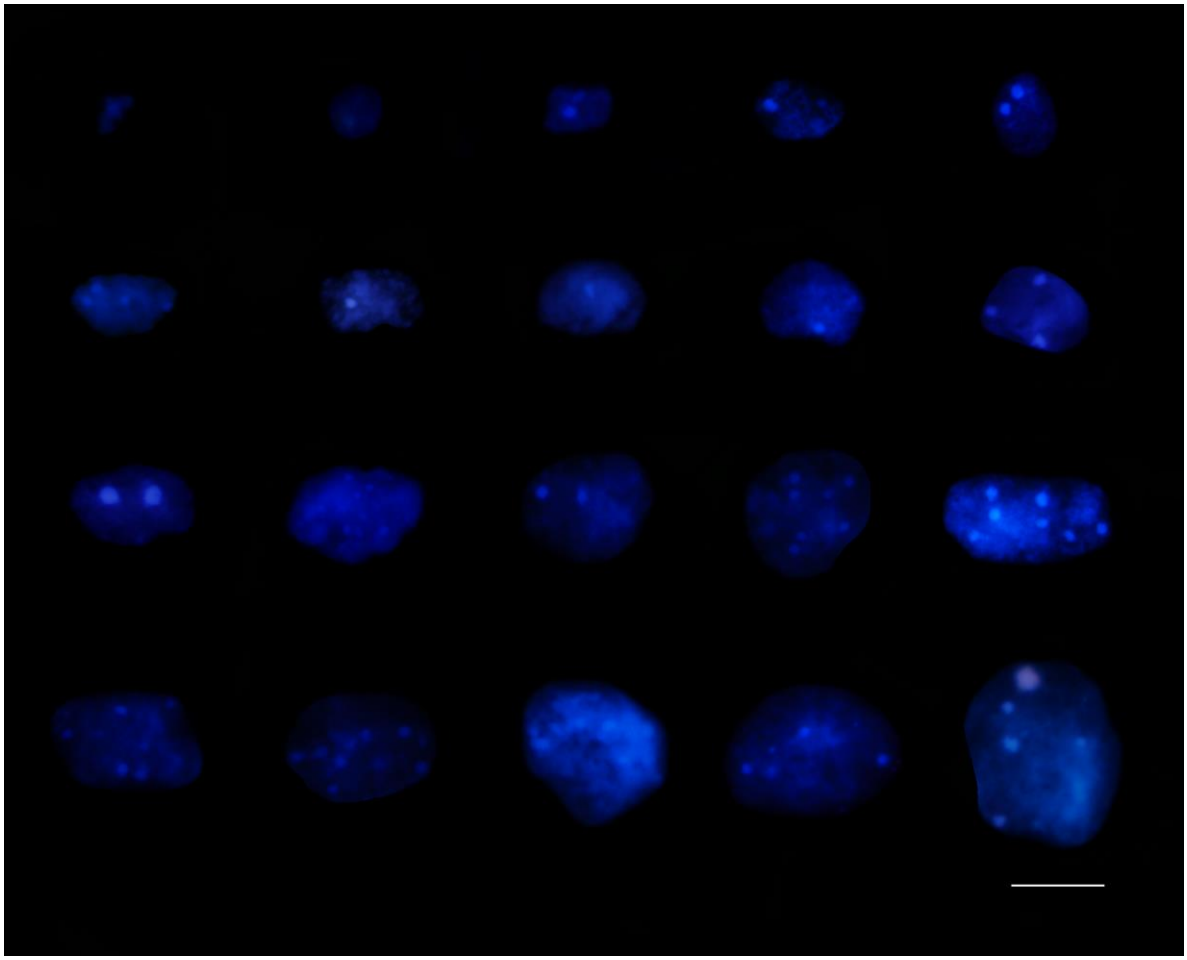

Figure 6. MN obtained from DAPI counterstaining showing the presence of AT rich-portions in the MN composition. A variation of positive DAPI signals were visualized in each MN. Also, each MN presented chromatin with different compaction level. Bar = 10 µm.

The micromanipulation procedure provided DNA fragments of the MN ranging from 100 – 1000 bp for MN 1, predominating 200 – 400 bp, and 100 – 2000 bp equally distributed for MN 2 (Supplementary Figure 1). Corroborating the previous data (MN DNA sizing and DNA sequence composition), the origin of these structures involved different chromosome fragments. Strong hybridization signals were visualized in all chromosomes (Figure 7). The MN 1 probe pool provided strong signals along the length of all chromosomes, with a lower accumulated profile in chromosome 6 and the short arm of chromosomes 2, 3, 4 and 9 (Figure 7a). The MN 2 probe pool showed intense spread signals along the length of all chromosomes except on centromeric, knob and secondary constriction regions (Figure 7b).

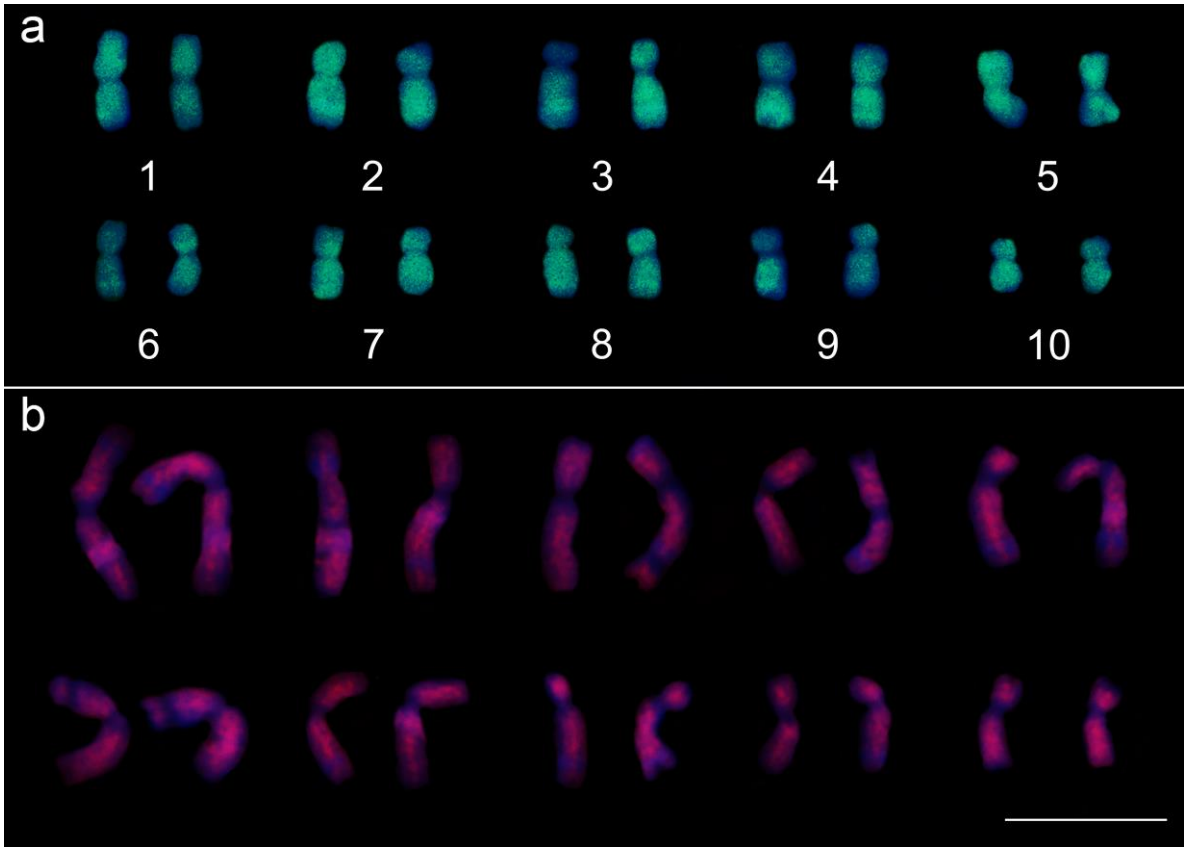

Figure 7. Mapping from MN probes labelled with **(a)** ChromaTide-488-5-dUTP (green) for MN 1 and **(b)** Tetramethyl-rhodamine 5-dUTP (red) for MN 2 in metaphase chromosomes of *Z. mays*. **(a)** The MN 1 probe pool resulted in accumulated hybridization signals along the chromosomes and less signals in chromosome 6 and the short arm of chromosomes 2, 3, 4 and 9. **(b)** The MN 2 probe pool showed intense spread signals over the chromosome length with exception of the centromeric, knob and secondary constriction regions. Bar = 10 µm.

4. Discussion

The MN varied in DNA sizing, composition based on variation of fluorescence signals of repetitive DNA sequences, and also origin, revealing the genotoxic impact of the MMS. The procedures employed here enabled the ascertainment of the DNA sizing, composition and origin of induced MN of *Z. mays*. Other mutagens (like N-nitroso-N-methylurea, maleic hydrazide and X-rays) also induced MN presenting different compositions in meristematic cells of *H. vulgare* (Juchimiuk et al., 2007) and *B. distachyon* (Kus et al., 2018). Different to our study, these authors showed

that the MN presented variations in the occurrence of centromeric, telomeric and/or rDNA gene sequences.

MN variability is a consequence of the action mechanism of MMS. MMS is a clastogenic and alkylating agent that promotes methylations in DNA nitrogenous bases. This mutagen acts by generating over 80% of its methyl adducts at the N7-guanine, 10% of this alkylation change at the N3-adenine and 0.3% at the O6-guanine (Jenkins et al., 2005). These purine bases occur along the *Z. mays* genome that contains 52.8% AT and 47.2% GC (Meister and Barow, 2007). Therefore, the MN with different DNA sizing, compositions and/or origins are consequence of the MMS damages on several genomic portions of the *Z. mays* genome.

Based on image cytometry data, the MN are distinct in relation to DNA sizing. Considering the nuclear 1C value of *Z. mays* 'AL Bandeirante' (1C = 2.983 x 10^9 bp, Silva et al., 2018), our results indicated that ~16.76% to 50.28% of this reference value was lost due to MN formation. Regarding the 1C value of each chromosome of *Z. mays* 'AL Bandeirante' (Silva et al., 2018), our data showed that the MN presented DNA sizing values equivalent to different chromosome fragments. Moreover, the MN that presented DNA sizing values between 2.0 – 3.0 pg were generated from genomic fragments of different chromosomes. The MMS overdose used here possibly potentialized the number of chromosome breaks, which were accumulated and delimited by the membrane of a single one cell, generating these MN with a high DNA sizing value. The MMS promotes a delay of the replication fork progression due to methylation at the N3-adenine (Tercero and Diffley, 2001; Chang et al., 2002), consequently leading to a slower S phase progression and an interference in the cell cycle. Thus, probably the majority of the MN evaluated here were observed in cells with 2C value.

All MN showed signals of the 180-bp knob and *Grande* LTR-retrotransposon sequences, in spite of the variation of fluorescence signals (number and/or intensity) among the MN. Until this study, centromeric, telomeric and rDNA sequences were used to analyze the composition of plant MN (Jovtchev et al., 2002; Juchimiuk et al., 2007; Juchimiuk-Kwasniewska et al., 2011; Kus et al., 2017; Kus et al., 2018). Our results evidenced that the MN is composed additionally of other DNA sequences, as the 180-bp knob and *Grande* LTR-retrotransposon sequences. From MN composition and chromosome mapping of the 180-bp knob sequence and $DAPI^+$

banding, we concluded that there are fragments of chromosomes 1, 2, 4, 5 and 8 in MN composition. In addition, the hybridization profile of *Grande* LTR-retrotransposon sequence confirmed the MN composition and also evidenced that the MN possess genomic sequences of other *Z. mays* chromosomes, since this *Grande* LTR-retrotransposon is distributed along the ten chromosomes. The 180-bp knob is rich in AT (Peacock et al., 1981; Jian et al., 2017) and the *Grande* LTR-retrotransposon presents 52% GC (García-Martínez and Martínez-Izquierdo, 2003; Sanmiguel and Vitte, 2009). As adenine and mainly guanine bases are targeted by MMS (Jenkins et al., 2005), these sequences can be indicated as hotspots of MMS DNA damage and consequently MN generation in *Z. mays*, mainly the *Grande* LTR-retrotransposon.

We reinforced this consideration based on results obtained from probes of the microdissected MN. The two-probe pools from microdissected MN showed hybridization signals in all chromosomes, evidencing that these MN were originated from fragments consisting of sequences common to all *Z. mays* chromosomes. In addition, the MN 1 and MN 2 possess *Grande* LTR-retrotransposon sequences, as this sequence is evenly distributed along the ten chromosomes of *Z. mays*. The preference of MMS for guanine (Jenkins et al., 2005) may have contributed to these results, since the *Grande* LTR-retrotransposon sequence is rich in GC portions (García-Martínez and Martínez-Izquierdo, 2003; Sanmiguel and Vitte, 2009). LTR-retrotransposons compose ~75% of the *Z. mays* 'B73' reference genome (Schnable et al., 2009). Besides the *Grande* LTR-retrotransposon of the *Gypsy* superfamily, there are other families of these mobile elements distributed throughout the *Z. mays* chromosomes, such as *Huck*, *Cinful*, *Tekay/Prem-1* (*Gypsy* superfamily) *Prem-2/Ji* and *Opie* of the *Copia* superfamily (Mroczek and Dawe, 2003; Lamb et al., 2007). In view of this, it is possible that the analyzed MN originated from fragments also containing sequences from these other retrotransposons.

The different MN presented variable number of specific signals for the 180-bp knob sequence and AT portions ($DAPI^+$). Considering that MMS introduces a methyl group to N3-adenine (Wyatt and Pittman, 2006), the presence of these signals is another consequence of the employed mutagen. Knobs are heterochromatic regions consisting of tandem repeat sequences integrated with LTR-retrotransposons (Ananiev et al., 1998; Lamb et al., 2007). Thus, the difference of heterochromatin

distribution among the MN may be correlated to the presence of these repetitive DNA sequences in MN composition.

The MN 1 and MN 2 were originated from different chromosome fragments, since the pattern of hybridization signals of each MN probe pool were distinct, confirming the distinct profiles exhibited by the DOP-PCR products. In the MN 1 probe pool, the fluorescence signals were often distributed along the ten chromosomes. Whereas the MN 2 probe pool did not show hybridization signals in centromeric, knob and secondary constriction regions.

5. Conclusions

Image cytometry and FISH with probes generated from repetitive DNA sequences and microdissected MN showed that MMS-induced MN of *Z. mays* are variable in DNA sizing, composition based on presence of 180-bp knob and *Grande* LTR-retrotransposon sequences, and origin. Fragments consisting of 180-bp knob and the *Grande* LTR-retrotransposon were highlighted as frequently involved in MN formation. In addition, the results are correlated to the mechanism of action of MMS, demonstrating the extent of the genotoxic damage promoted by the MMS mutagen in the *Z. mays* genome.

6. Acknowledgments

We would like to thank the Conselho Nacional de Desenvolvimento Científico e Tecnológico (CNPq, Brasília – DF, Brazil) and the Coordernação de Aperfeiçoamento de Pessoal de Nível Superior (CAPES, Brasília – DF, Brazil) – Finance Code 001 for providing the financial support for this study.

7. References

Alvarenga, I.F.S., dos Santos, F.E., Silveira, G.L., Andrade-Vieira, L.F., Martins, G.C., Guilherme, L.R.G., 2020. Investigating arsenic toxicity in tropical soils: A cell cycle and DNA fragmentation approach. Sci. Total Environ. 698, 134272. https://doi.org/10.1016/j.scitotenv.2019.134272

Ananiev, E. V, Phillips, R.L., Rines, H.W., 1998. Complex Structure of Knob DNA on Maize Chromosome 9 : Retrotransposon Invasion into Heterochromatin 10.

Bhering, L.L., 2017. Rbio: A tool for biometric and statistical analysis using the R platform. Crop Breed. Appl. Biotechnol. 17, 187–190. https://doi.org/10.1590/1984-70332017v17n2s29

Böcking, A., Huy Nguyen, V.Q., 2004. Diagnostic and Prognostic Use of DNA Image Cytometry in Cervical Squamous Intraepithelial Lesions and Invasive Carcinoma. Cancer 102, 41–54. https://doi.org/10.1002/cncr.11889

Caritá, R., Marin-Morales, M.A., 2008. Induction of chromosome aberrations in the *Allium cepa* test system caused by the exposure of seeds to industrial effluents contaminated with azo dyes. Chemosphere 72, 722–725. https://doi.org/10.1016/j.chemosphere.2008.03.056

Carvalho, C.R., Clarindo, W.R., Abreu, I.S., 2011. Image cytometry: nuclear and chromosomal DNA quantification. Methods Mol. Biol. 689, 51–68. https://doi.org/10.1007/978-1-60761-950-5_4

Chang, M., Bellaoui, M., Boone, C., Brown, G.W., 2002. A genome-wide screen for methyl methanesulfonate-sensitive mutants reveals genes required for S phase progression in the presence of DNA damage. Proc. Natl. Acad. Sci. U. S. A. 99, 16934–16939. https://doi.org/10.1073/pnas.262669299

Chen, L., Yuan, S., Liu, X., Zhou, X., Zhou, Y., Song, Y., 2020. Genotoxicity response of *Vicia faba* seedlings to cadmium in soils as characterized by direct soil exposure and micronucleus test. Ecotoxicology 29, 65–74. https://doi.org/10.1007/s10646-019-02138-7

Chung, H.W., Kang, S.J., Kim, S.Y., 2002. A combination of the micronucleus assay and a FISH technique for evaluation of the genotoxicity of 1,2,4-benzenetriol. Mutat. Res. - Genet. Toxicol. Environ. Mutagen. 516, 49–56. https://doi.org/10.1016/S1383-5718(02)00018-9

De Grippa, G.A., Morozesk, M., Nati, N., Matsumoto, S.T., 2010. Estudo genotoxico do surfactante Tween 80 em *Allium cepa*. Rev. Bras. Toxicol. 23, 11–16.

Doležel, J., Greilhuber, J., Suda, J., 2007. Estimation of nuclear DNA content in plants using flow cytometry. Nat. Protoc. 2, 2233–2244. https://doi.org/10.1038/nprot.2007.310

Engelen, J.J.M., Albrechts, J.C.M., Hamers, G.J.H., Geraedts, J.P.M., 1998. A

simple and efficient method for microdissection and microFISH. J. Med. Genet. 35, 265–268. https://doi.org/10.1136/jmg.35.4.265

Fauth, E., Scherthan, H., Zankl, H., 2000. Chromosome painting reveals specific patterns of chromosome occurrence in mitomycin C- and diethylstilboestrol-induced micronuclei. Mutagenesis 15, 459–467. https://doi.org/10.1093/mutage/15.6.459

Fenech, M., Kirsch-Volders, M., Natarajan, A.T., Surralles, J., Crott, J.W., Parry, J., Norppa, H., Eastmond, D.A., Tucker, J.D., Thomas, P., 2011. Molecular mechanisms of micronucleus, nucleoplasmic bridge and nuclear bud formation in mammalian and human cells. Mutagenesis 26, 125–132. https://doi.org/10.1093/mutage/geq052

Fimognari, C., Sauer-Nehls, S., Braselmann, H., Nüsse, M., 1997. Analysis of radiation-induced micronuclei by FISH using a combination of painting and centromeric DNA probes. Mutagenesis 12, 91–95. https://doi.org/10.1093/mutage/12.2.91

Fourastié, M.F., Gottlieb, A.M., Poggio, L., González, G.E., 2018. Are cytological parameters of maize landraces (*Zea mays* ssp. mays) adapted along an altitudinal cline? J. Plant Res. 131, 285–296. https://doi.org/10.1007/s10265-017-0996-3

García-Martínez, J., Martínez-Izquierdo, J.A., 2003. Study on the evolution of the *Grande* retrotransposon in the *Zea* genus. Mol. Biol. Evol. 20, 831–841. https://doi.org/10.1093/molbev/msg095

Gieni, R.S., Chan, G.K.T., Hendzel, M.J., 2008. Epigenetics regulate centromere formation and kinetochore function. J. Cell. Biochem. 104, 2027–2039. https://doi.org/10.1002/jcb.21767

Gisselsson, D., 2008. Classification of chromosome segregation errors in cancer. Chromosoma 117, 511–519. https://doi.org/10.1007/s00412-008-0169-1

Gregory, T. R., 2021. Animal Genome Size Database. http://www.genomesize.com

Greilhuber, J., 2008. Cytochemistry and C-values: The less-well-known world of nuclear DNA amounts. Ann. Bot. 101, 791–804. https://doi.org/10.1093/aob/mcm250

Guo, X., Ni, J., Liang, Z., Xue, J., Fenech, M.F., Wang, X., 2019. The molecular origins and pathophysiological consequences of micronuclei: New insights into an age-old problem. Mutat. Res. - Rev. Mutat. Res. 779, 1–35. https://doi.org/10.1016/j.mrrev.2018.11.001

Guttenbach, M., Schmid, M., 1994. Exclusion of specific human chromosomes into micronuclei by 5-azacytidine treatment of lymphocyte cultures. Exp. Cell Res. https://doi.org/10.1006/excr.1994.1068

Hardie, D.C., Gregory, T.R., Hebert, P.D.N., 2002. From pixels to picograms: A beginners' guide to genome quantification by Feulgen image analysis densitometry. J. Histochem. Cytochem. 50, 735–749. https://doi.org/10.1177/002215540205000601

Haroske, G., Baak, J.P.A., Danielsen, H., Giroud, F., Gschwendtner, A., Oberholzer, M., Reith, A., Spieler, P., Böcking, A., 2001. Fourth updated ESACP consensus report on diagnostic DNA image cytometry. Anal. Cell. Pathol. 23, 89–95. https://doi.org/10.1155/2001/657642

Heit, R., Rattner, J.B., Chan, G.K.T., Hendzel, M.J., 2009. G2 histone methylation is required for the proper segregation of chromosomes. J. Cell Sci. 122, 2957–2968. https://doi.org/10.1242/jcs.045351

Hintzsche, H., Hemmann, U., Poth, A., Utesch, D., Lott, J., Stopper, H., 2017. Fate of micronuclei and micronucleated cells. Mutat. Res. - Rev. Mutat. Res. 771, 85–98. https://doi.org/10.1016/j.mrrev.2017.02.002

Hovhannisyan, G., Aroutiounian, R., Liehr, T., 2012. Chromosomal Composition of Micronuclei in Human Leukocytes Exposed to Mitomycin C. J. Histochem. Cytochem. 60, 316–322. https://doi.org/10.1369/0022155412436587

Itoh, S., Hattori, C., 2019. In vivo genotoxicity of 1,4-dioxane evaluated by liver and bone marrow micronucleus tests and Pig-a assay in rats. Mutat. Res. - Genet. Toxicol. Environ. Mutagen. 837, 8–14. https://doi.org/10.1016/j.mrgentox.2018.09.004

Jenkins, G.J.S., Doak, S.H., Johnson, G.E., Quick, E., Waters, E.M., Parry, J.M., 2005. Do dose response thresholds exist for genotoxic alkylating agents? Mutagenesis 20, 389–398. https://doi.org/10.1093/mutage/gei054

Jian, Y., Xu, C., Guo, Z., Wang, S., Xu, Y., Zou, C., 2017. Maize (*Zea mays* L.) genome size indicated by 180-bp knob abundance is associated with flowering time. Sci. Rep. 7, 1–9. https://doi.org/10.1038/s41598-017-06153-8

Jovtchev, G., Stergios, M., Schubert, I., 2002. A comparison of N-methyl-N-nitrosourea-induced chromatid aberrations and micronuclei in barley meristems using FISH techniques. Mutat. Res. - Genet. Toxicol. Environ. Mutagen. 517, 47–51. https://doi.org/10.1016/S1383-5718(02)00038-4

Juchimiuk-Kwasniewska, J., Brodziak, L., Maluszynska, J., 2011. FISH in analysis of gamma ray-induced micronuclei formation in barley. J. Appl. Genet. 52, 23–29. https://doi.org/10.1007/s13353-010-0017-x

Juchimiuk, J., Hering, B., Maluszynska, J., 2007. Multicolour FISH in an analysis of chromosome aberrations induced by N-nitroso-N-methylurea and maleic hydrazide in barley cells. J. Appl. Genet. 48, 99–106. https://doi.org/10.1007/BF03194666

Kirsch-Volders, M., Plas, G., Elhajouji, A., Lukamowicz, M., Gonzalez, L., Vande

Loock, K., Decordier, I., 2011. The in vitro MN assay in 2011: Origin and fate, biological significance, protocols, high throughput methodologies and toxicological relevance. Arch. Toxicol. 85, 873–899. https://doi.org/10.1007/s00204-011-0691-4

Kus, A., Kwasniewska, J., Hasterok, R., 2017. *Brachypodium distachyon* - A useful model in the qualification of mutagen-induced micronuclei using multicolor FISH. PLoS One 12, 1–13. https://doi.org/10.1371/journal.pone.0170618

Kus, A., Kwasniewska, J., Szymanowska-Pułka, J., Hasterok, R., 2018. Dissecting the chromosomal composition of mutagen-induced micronuclei in *Brachypodium distachyon* using multicolour FISH. Ann. Bot. 122, 1161–1171. https://doi.org/10.1093/aob/mcy115

Kus, A., Szymanowska-Pułka, J., Kwasniewska, J., Hasterok, R., 2019. Detecting *Brachypodium distachyon* chromosomes Bd4 and Bd5 in MH- and X-ray-induced micronuclei using mcFISH. Int. J. Mol. Sci. 20. https://doi.org/10.3390/ijms20112848

Lamb, J.C., Meyer, J.M., Corcoran, B., Kato, A., Han, F., Birchler, J.A., 2007. Distinct chromosomal distributions of highly repetitive sequences in maize. Chromosom. Res. 15, 33–49. https://doi.org/10.1007/s10577-006-1102-1

Lee, S.-I., Kim, N.-S., 2014. Transposable elements and genome size variations in plants. Genomics Inform. 12, 87. https://doi.org/10.5808/GI.2014.12.3.87

Leme, D.M., Marin-Morales, M.A., 2008. Chromosome aberration and micronucleus frequencies in *Allium cepa* cells exposed to petroleum polluted water-A case study. Mutat. Res. - Genet. Toxicol. Environ. Mutagen. 650, 80–86. https://doi.org/10.1016/j.mrgentox.2007.10.006

Leveroni, F.A., Caffetti, J.D., Pastori, M.C., 2017. Genotoxic response of blood, gill and liver cells of *Piaractus mesopotamicus* after an acute exposure to a glyphosate-based herbicide. Caryologia 70, 21–28. https://doi.org/10.1080/00087114.2016.1254454

Lima, M.G.F., Rocha, L.C., Silveira, G.L., Alvarenga, I.F.S., Andrade-Vieria, L.F., 2019. Nucleolar alterations are reliable parameters to determine the cytogenotoxicity of environmental pollutants. Ecotoxicol. Environ. Saf. 174, 630–636. https://doi.org/10.1016/j.ecoenv.2019.03.033

Lundin, C., North, M., Erixon, K., Walters, K., Jenssen, D., Goldman, A.S.H., Helleday, T., 2005. Methyl methanesulfonate (MMS) produces heat-labile DNA damage but no detectable in vivo DNA double-strand breaks. Nucleic Acids Res. 33, 3799–3811. https://doi.org/10.1093/nar/gki681

Lysák, M.A., Schubert, I., 2013. Mechanisms of chromosome rearrangements in Greilhuber, J., Dolezel, J., Wendel, J.F. (Eds.), Plant Genome Diversity. Springer, Vienna, pp. 137-147.

Meister, A., Barow, M., 2007. DNA Base Composition of Plant Genomes, Flow Cytometry with Plant Cells: Analysis of Genes, Chromosomes and Genomes. https://doi.org/10.1002/9783527610921.ch8

Miller, B.M., Nússe, M., 1993. Analysis of micronuclei induced by 2-chlorobenzylidene malonitrile (CS) using fluorescence *in situ* hybridization with telomeric and centromeric DNA probes, and flow cytometry. Mutagenesis 8, 35–41. https://doi.org/10.1093/mutage/8.1.35

Mroczek, R.J., Dawe, R.K., 2003. Distribution of retroelements in centromeres and neocentromeres of maize. Genetics 165, 809–819.

Nüsse, M., Kramer, J., Miller, B.M., 1992. Factors influencing the DNA content of radiation-induced micronuclei. Int. J. Radiat. Biol. 62, 587–602. https://doi.org/10.1080/09553009214552511

Nüsse, M., Miller, B.M., Viaggi, S., Grawé, J., 1996. Analysis of the DNA content distribution of micronuclei using flow sorting and fluorescent *in situ* hybridization with a centromeric DNA probe. Mutagenesis 11, 405–413. https://doi.org/10.1093/mutage/11.4.405

Peace, B.E., Livingston, G., Silberstein, E.B., Loper, J.C., 1999. A case of elevated spontaneous micronucleus frequency derived from chromosome 2. Mutat. Res. - Fundam. Mol. Mech. Mutagen. 430, 109–119. https://doi.org/10.1016/S0027-5107(99)00171-2

Peacock, W.J., Dennis, E.S., Rhoades, M.M., Pryor, A.J., 1981. Highly repeated DNA sequence limited to knob heterochromatin in maize. Proc. Natl. Acad. Sci. 78, 4490–4494. https://doi.org/10.1073/pnas.78.7.4490

Pellicer, J., Leitch, I.J., 2020. The Plant DNA C-values database (release 7.1): an updated online repository of plant genome size data for comparative studies. New Phytol. 226, 301–305. https://doi.org/10.1111/nph.16261

Rodenacker, K., Bengtsson, E., 2003. A feature set for cytometry on digitized microscopic images. Anal. Cell. Pathol. 25, 1–36. https://doi.org/10.1155/2003/548678

Sanmiguel, P., Vitte, C., 2009. The LTR-retrotransposons of maize. Handb. Maize Genet. Genomics 9780387778, 307–327. https://doi.org/10.1007/978-0-387-77863-1_15

Schnable, P.S., Ware, D., Fulton, R.S., Stein, J.C., Wei, F., Pasternak, S., Liang, C., Zhang, J., Fulton, L., Graves, T.A., Minx, P., Reily, A.D., Courtney, L., Kruchowski, S.S., Tomlinson, C., Strong, C., Delehaunty, K., Fronick, C., Courtney, B., Rock, S.M., Belter, E., Du, F., Kim, K., Abbott, R.M., Cotton, M., Levy, A., Marchetto, P., Ochoa, K., Jackson, S.M., Gillam, B., Chen, W., Yan, L., Higginbotham, J., Cardenas, M., Waligorski, J., Applebaum, E., Phelps, L., Falcone, J., Kanchi, K., Thane, T., Scimone, A., Thane, N., Henke, J., Wang, T., Ruppert, J., Shah, N., Rotter, K., Hodges, J., Ingenthron, E., Cordes, M.,

Kohlberg, S., Sgro, J., Delgado, B., Mead, K., Chinwalla, A., Leonard, S., Crouse, K., Collura, K., Kudrna, D., Currie, J., He, R., Angelova, A., Rajasekar, S., Mueller, T., Lomeli, R., Scara, G., Ko, A., Delaney, K., Wissotski, M., Lopez, G., Campos, D., Braidotti, M., Ashley, E., Golser, W., Kim, H., Lee, S., Lin, J., Dujmic, Z., Kim, W., Talag, J., Zuccolo, A., Fan, C., Sebastian, A., Kramer, M., Spiegel, L., Nascimento, L., Zutavern, T., Miller, B., Ambroise, C., Muller, S., Spooner, W., Narechania, A., Ren, L., Wei, S., Kumari, S., Faga, B., Levy, M.J., McMahan, L., Van Buren, P., Vaughn, M.W., Ying, K., Yeh, C.T., Emrich, S.J., Jia, Y., Kalyanaraman, A., Hsia, A.P., Barbazuk, W.B., Baucom, R.S., Brutnell, T.P., Carpita, N.C., Chaparro, C., Chia, J.M., Deragon, J.M., Estill, J.C., Fu, Y., Jeddeloh, J.A., Han, Y., Lee, H., Li, P., Lisch, D.R., Liu, S., Liu, Z., Nagel, D.H., McCann, M.C., Sanmiguel, P., Myers, A.M., Nettleton, D., Nguyen, J., Penning, B.W., Ponnala, L., Schneider, K.L., Schwartz, D.C., Sharma, A., Soderlund, C., Springer, N.M., Sun, Q., Wang, H., Waterman, M., Westerman, R., Wolfgruber, T.K., Yang, L., Yu, Y., Zhang, L., Zhou, S., Zhu, Q., Bennetzen, J.L., Dawe, R.K., Jiang, J., Jiang, N., Presting, G.G., Wessler, S.R., Aluru, S., Martienssen, R.A., Clifton, S.W., McCombie, W.R., Wing, R.A., Wilson, R.K., 2009. The B73 maize genome: Complexity, diversity, and dynamics. Science (80-.). 326, 1112–1115. https://doi.org/10.1126/science.1178534

Schubert, I., Rieger, R., Fuchs, J., Pich, U., 1994. Sequence organization and the mechanism of interstitial deletion clustering in a plant genome (*Vicia faba*). Mutat. Res. Lett. 325, 1–5. https://doi.org/10.1016/0165-7992(94)90020-5

Schwarzacher, T., Heslop-Harrison, P., 2000. Practical *in situ* hybridization, BIOS Scientific Publishers Ltd, Oxford.

Silva, J.C., Carvalho, C.R., Clarindo, W.R., 2018. Updating the maize karyotype by chromosome DNA sizing. PLoS One 13, 1–13. https://doi.org/10.1371/journal.pone.0190428

Silva, J.C., Soares, F.A.F., Sattler, M.C., Clarindo, W.R., 2020. Repetitive sequences and structural chromosome alterations promote intraspecific variations in *Zea mays* L. karyotype. Sci. Rep. 10, 1–9. https://doi.org/10.1038/s41598-020-65779-3

Soares, F.A.F., Carvalho, C.R., Sattler, M.C., Silva, J.C., Pinto, D.E.E., Passamani, P.Z., Silva, A.J., Clarindo, W.R., 2020. Plant Chromosome-Specific Probes by Microdissection of a Single Chromosome: Is That a Reality? Front. Plant Sci. 11, 1–9. https://doi.org/10.3389/fpls.2020.00334

Telenius, Håk., Ponder, B.A.J., Tunnacliffe, A., Pelmear, A.H., Carter, N.P., Ferguson-Smith, M.A., Behmel, A., Nordenskjöld, M., Pfragner, R., 1992. Cytogenetic analysis by chromosome painting using dop-pcr amplified flow-sorted chromosomes. Genes, Chromosom. Cancer 4, 257–263. https://doi.org/10.1002/gcc.2870040311

Tercero, J.A., Diffley, J.F.X., 2001. Regulation of DNA replication fork progression through damaged DNA by the Mec1/Rad53 checkpoint. Nature 412, 553–557. https://doi.org/10.1038/35087607

Terradas, M., Martín, M., Tusell, L., Genescà, A., 2010. Genetic activities in micronuclei: Is the DNA entrapped in micronuclei lost for the cell? Mutat. Res. - Rev. Mutat. Res. 705, 60–67. https://doi.org/10.1016/j.mrrev.2010.03.004

Vilhar, B., Greilhuber, J., Koce, J.D., Temsch, E.M., Dermastia, M., 2001. Plant genome size measurement with DNA image cytometry. Ann. Bot. 87, 719–728. https://doi.org/10.1006/anbo.2001.1394

Wang, C.J.R., Harper, L., Cande, W.Z., 2006. High-resolution single-copy gene fluorescence in situ hybridization and its use in the construction of a cytogenetic map of maize chromosome 9. Plant Cell 18, 529–544. https://doi.org/10.1105/tpc.105.037838

Wang, J., Che, B., Zhang, L.W., Dong, G., Luo, Q., Xin, L., 2017. Comparative genotoxicity of silver nanoparticles in human liver HepG2 and lung epithelial A549 cells. J. Appl. Toxicol. 37, 495–501. https://doi.org/10.1002/jat.3385

Wyatt, M.D., Pittman, D.L., 2006. Methylating agents and DNA repair responses: Methylated bases and sources of strand breaks. Chem. Res. Toxicol. 19, 1580–1594. https://doi.org/10.1021/tx060164e

Yang, F., Trifonov, V., Ng, B.L., Kosyakova, N., Carter, N.P., 2017. Generation of Paint Probes from Flow-Sorted and Microdissected Chromosomes 63–79. https://doi.org/10.1007/978-3-662-52959-1_6

Zyss, D., Gergely, F., 2009. Centrosome function in cancer: guilty or innocent? Trends Cell Biol. 19, 334–346. https://doi.org/10.1016/j.tcb.2009.04.001

8. Supplementary Material

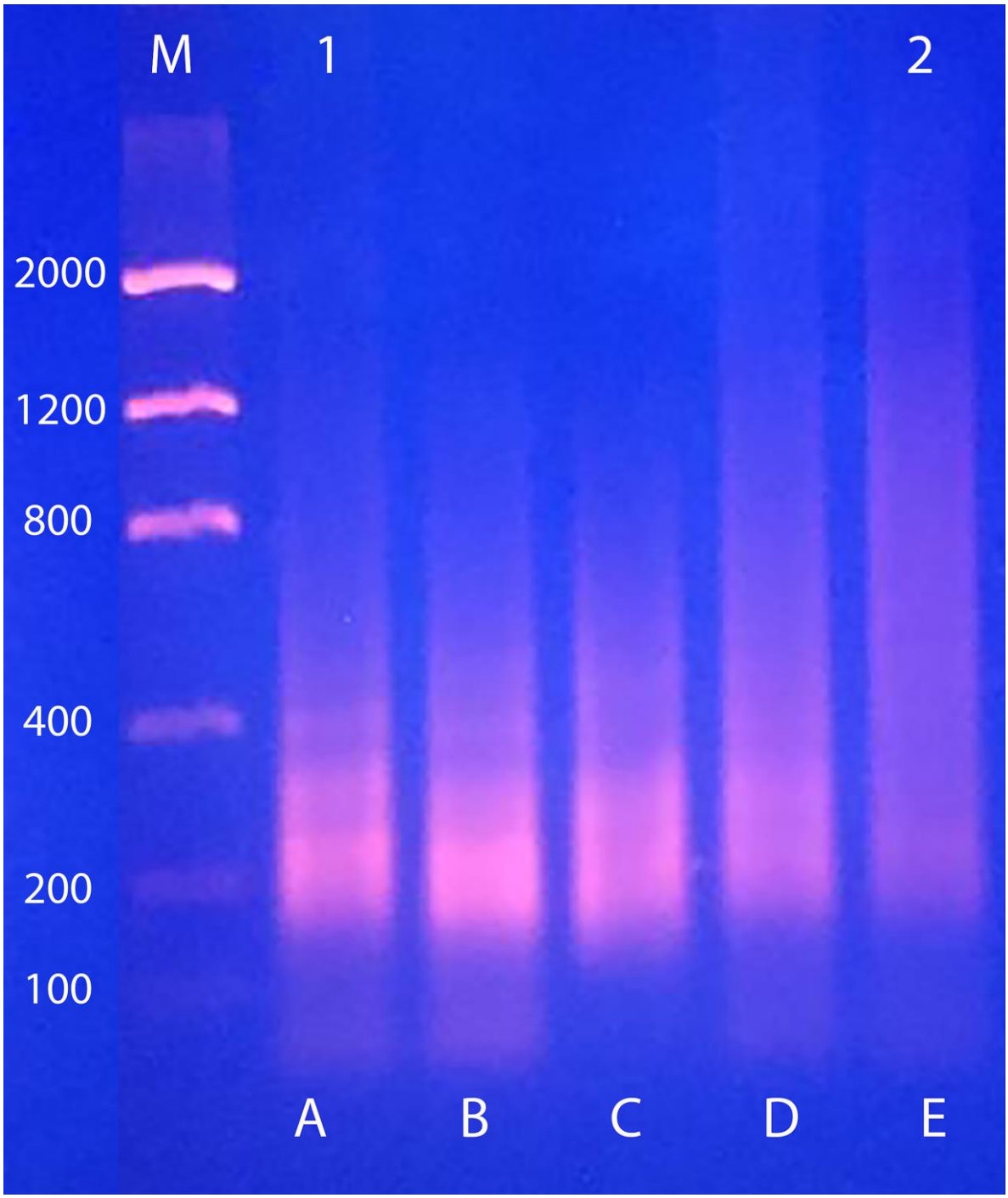

Supplementary Figure 1. DOP-PCR amplification products of the five microdissected MN A, B, C, D and E analyzed in 1.5% agarose gel. Line M represents the base pair marker and lines 1 and 2 indicate the amplification products that resulted from microdissected MN 1 and MN 2, respectively.

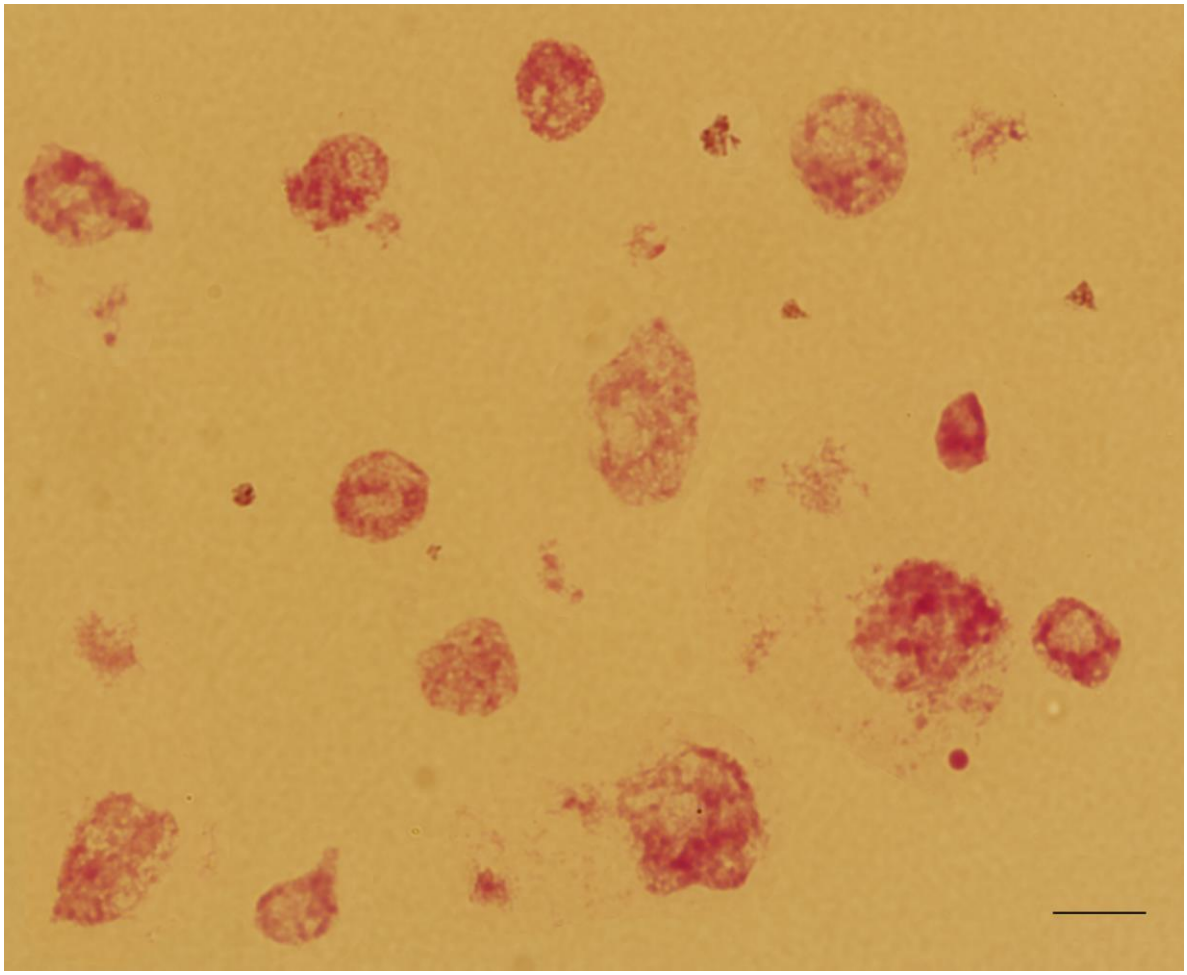

Supplementary Figure 2. Stoichiometrically stained nuclei and MN of *Z. mays* obtained from slides submitted to hydrolysis with 5 M HCl for 45 min and stained with Schiff's reagent for 12 h. Bar = 10 µm.

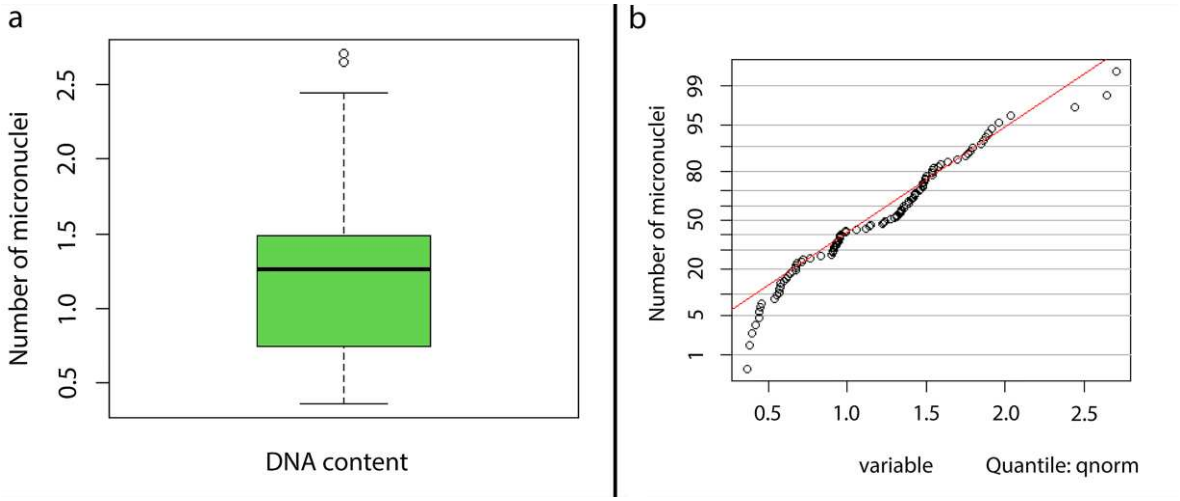

Supplementary Figure 3. (a) Boxplot and **(b)** probplot graphics presenting the dispersion of MN DNA values in pg.